Supporting Information (SI)

Exploring Interactions of Aptamers with $A\beta_{40}$ Amyloid Aggregates and Its Application: Detection of Amyloid Aggregates

Yan Zheng,[†] Xiuhua Geng,[†] Xiaohai Yang,[†] Shaoyuan Li,[†] Yaqin Liu,[†] Xiaofeng Liu,[†] Qing Wang,*,[†] Kemin Wang,*,[†] Ruichen Jia[†] and Yao Xu[§]

[†]State Key Laboratory of Chemo/Biosensing and Chemometrics, College of Chemistry and Chemical Engineering, Key Laboratory for Bio-Nanotechnology and Molecular Engineering of Hunan Province, Hunan University, Changsha 410082, P. R. China

[§]Huaihe Hospital of Henan University, Henan University, Kaifeng 475000, P. R. China

* *Correspondence to author: Qing Wang and Kemin Wang, E-mail: wwqq99@hnu.edu.cn; kmwang@hnu.edu.cn. Tel/Fax: +86-731-88821566.*

Table of contents

S-1 Materials and Reagents

DNA Apts (Apt1 and Apt2, the sequences in the Table S1) screened by Tsukakoshi et al[1] and random DNA (random DNA1 and random DNA2) were synthesized by Sangon Biotech Co., Ltd (Shanghai, China). $A\beta_{40}$ and $A\beta_{42}$ were provided from GL Biochem Ltd. (Shanghai, China). 1,1,1,3,3,3-Hexafluoroisopropanol (HFIP) was bought from Shanghai Macklin Biochemical Co., Ltd. (Shanghai, China). (3-Mercaptopropyl) trimethoxysilane (MPTMS) and N-Hydroxysuccinimide-polyethylenglycol-maleimide (NHS-PEG-MAL) were respectively obtained from Sigma (USA) and Nanocs (USA). Chloroauric acid ($HAuCl_4 \cdot 4H_2O$) and trisodium citrate dihydrate were provided by Shanghai Reagent Company (Shanghai, China) and Biochem Ltd. (Shanghai, China), respectively. 11-Mercapto-1-undecanol (MCU) and sodium dodecyl sulfate (SDS) were purchased from Sigma (USA).

Table S1. Sequences of all nucleic acid probes used.

Name	Sequence (5′-3′)
Aptamer1 (Apt1)	NH_2-GCT GCC TGT GGT GTT GGG GCG GGT GCG
	SH-(T)5-GCT GCC TGT GGT GTT GGG GCG GGT GCG
Aptamer2 (Apt2)	NH_2-GGT GGC TGG AGG GGG CGC GAA CG
	SH-(A)6-GGT GGC TGG AGG GGG CGC GAA CG
Random DNA1	CAC CCC ACC TCG CTC CCG TGA CAC TAA TGC TA-SH
Random DNA2	SH-TTTTTTTTTTTTTAACTATACAAC

S-2 Preparation and characterization of $A\beta_{40}$ aggregates

$A\beta_{40}$ powder was treated according to the previous work.[2, 3] Briefly, 400 μM $A\beta_{40}$ monomer stock solution was firstly obtained after $A\beta_{40}$ lyophilized powder completely dissolved in 1% ammonium solution. Then, for $A\beta_{40}$ oligomer, the stock monomer was diluted with PBS buffer (50 mM, pH 7.4) and incubated at 37 ^{o}C with shaking (300 rpm) for 2 hours. When the incubation time was 1 day, the $A\beta_{40}$ fibril could be prepared. Here, the concentration of Aβ aggregates was defined using UV-vis spectra,[4] and the concentration was calculated as equivalent concentrations to Aβ monomer.

AFM imaging was used to characterize $A\beta_{40}$ and $A\beta_{42}$ aggregates. 10 μL diluted Aβ sample with final concentration of 1 μM was pipetted on the freshly cleaved mica, then it was dried at room temperature. Subsequently, AFM images were obtained using SP13800N-SPA400 (Japan) with the PPP-SEIHR probe at dynamic force mode and the pixel of 512 × 512. Meanwhile, the analysis of size distribution of $A\beta_{40}$ aggregates was performed by dynamic-light-scattering (DLS) measurements, which was conducted on a Malvern Zetasizer Nano ZS system (Malvern Instruments; Worcestershire, UK) at 25 ^{o}C. After analysis using the in-built software of the instrument, the hydrodynamic diameters of of $A\beta_{40}$ aggregates were acquired.

The morphology of $A\beta_{40}$ aggregates was visualized using AFM imaging. As shown in Figure S1A, when $A\beta_{40}$ monomer was incubated for 2 h, heterogeneous and spherical $A\beta_{40}$ oligomers were distributed uniformly in mica surface with the average height of 8.9-18.3 nm (Figure S1B). After $A\beta_{40}$ monomer was incubated for 24 h, flexible branched $A\beta_{40}$ fibrils with diameters ranging from 2.2 to 4.7 nm were observed

(Figure S1D and Figure S1E). The results on the morphology of Aβ40 aggregates was consistent with the previous work.[3] Simultaneously, Figure S1C and Figure S1F demonstrated that mean hydrodynamic diameter of Aβ40 fibril (532.1 ± 9.4 nm) was larger than that of Aβ40 oligomer (27.4 ± 3.5 nm). The DLS results showed the Aβ40 aggregates were successfully obtained.

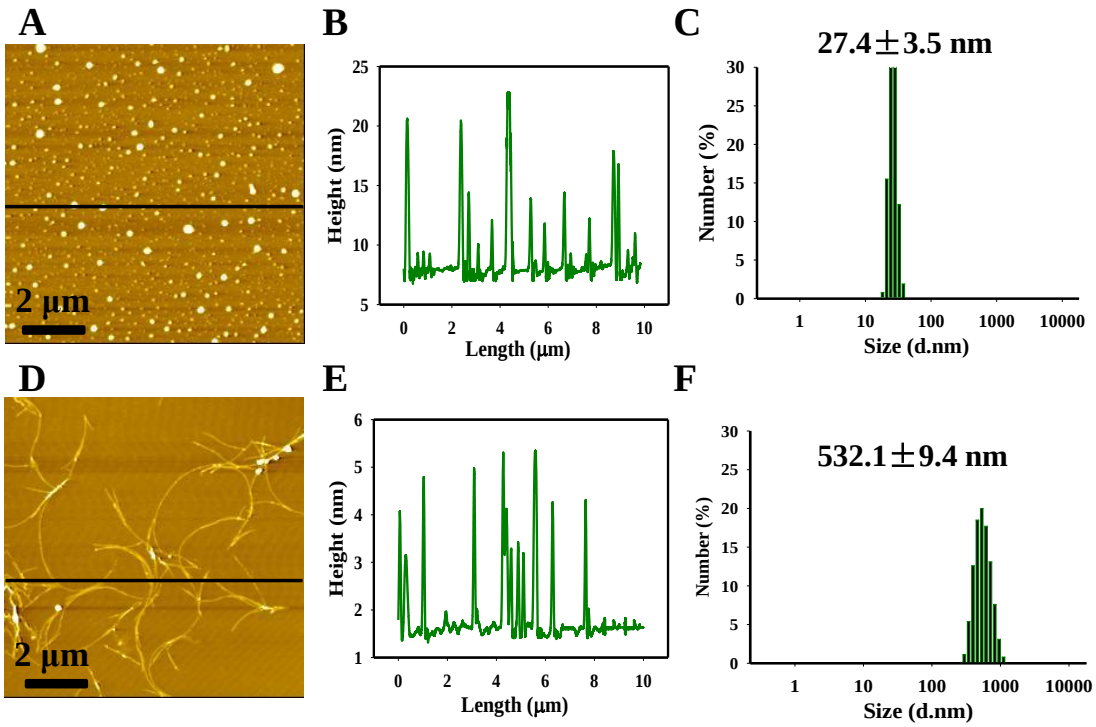

Figure S1. AFM images of Aβ40 oligomer (A), Aβ40 fibril (D). (B, E) The cross section profile along the black line in (A, D) shows the average height. The bar is 2 μm. The mean hydrodynamic diameter distributions of Aβ40 oligomer (C) and Aβ40 fibril (F).

S-3 Characterization of the immobilization of $A\beta_{40}$ aggregates on the Au film

Surface plasmon resonance (SPR) spectrometer was used to characterize the immobilization of $A\beta_{40}$ aggregates on Au film. Take the modification of $A\beta_{40}$ oligomer on the Au substrate for example, when the bare Au film was incubated with 200 nM $A\beta_{40}$ oligomer, the change of resonance angle was 0.0514° (shown in Figure S2). Since the resonance angle shift larger than 0.0015° was regarded as signal for the SPR instrument, the result indicated that the $A\beta_{40}$ aggregates could be modified on the Au film.

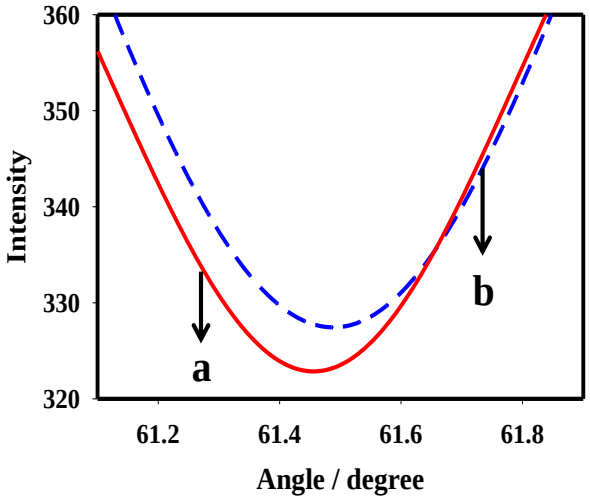

Figure S2. The SPR spectra of (a) the bare Au film and (b) $A\beta_{40}$ oligomer modified Au film.

S-4 Preparation and characterization of AuNPs and Apt1 functionalized AuNPs

AuNPs of 13 nm in diameter were prepared by the classical method of citrate reduction of $HAuCl_4$.[5] Apt functionalized AuNPs were prepared according to the literature with minor modifications.[6, 7]

UV-visible absorption spectra were used for optical characterization of bare AuNPs and Apt1 functionalized AuNPs in solution. As shown in Figure S3A, the absorption spectrum of AuNPs showed one peak at about 518.0 nm, while that of Apt1 functionalized AuNPs showed one peak at about 524.0 nm, indicating successful assembly of Apt1 on AuNPs. In this work, the absorbance (A = 0.54) of the diluted solution containing functionalized AuNPs remained unchanged, which indicated the concentration of functionalized AuNPs (2 nM) was constant. In addition, as shown in Figure S3B, the mean hydrodynamic diameter of AuNPs was 14.3 ± 1.3 nm. The mean hydrodynamic diameter of Apt1 functionalized AuNPs was 23.4 ± 1.8 nm, which implied successful modification of Apt1 on AuNPs.

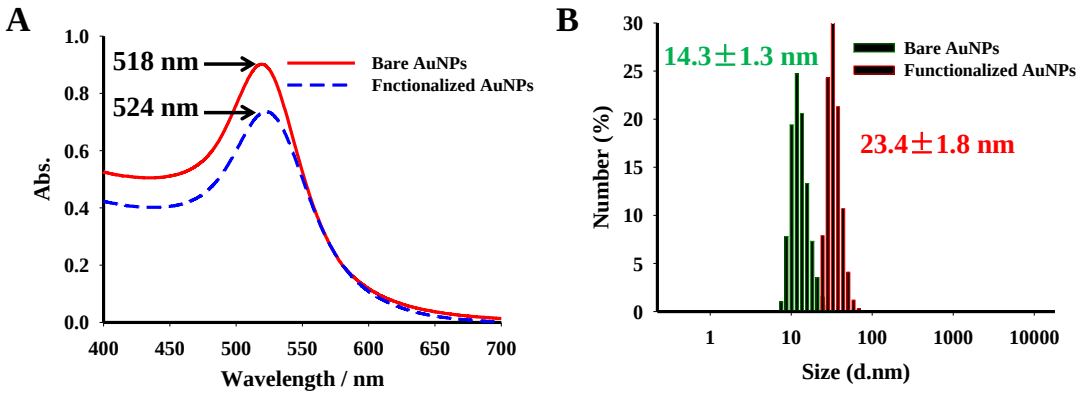

Figure S3. (A) UV-vis spectra of bare AuNPs (red; solid), and Apt1 functionalized AuNPs (blue; long dash). (B) The mean hydrodynamic diameter distributions of bare AuNPs (green column) and Apt1 functionalized AuNPs (red column).

S-5 Specificity of the interaction between Apts and $A\beta_{40}$ aggregates

A series of blocking experiments and control experiments were performed to characterize the specificity of interaction of aptamers (Apts) and $A\beta_{40}$ aggregates. As shown in Figure S4A, the binding probability of Apt1-$A\beta_{40}$ oligomer was 24.2% (blue, pillar I). When the $A\beta_{40}$ oligomer modified Au film was blocked by Apt1, the binding probability of Apt1 modified AFM tip-Apt1 blocked $A\beta_{40}$ oligomer modified Au film decreased clearly to 3.8% (blue, pillar II). When Apt1 modified AFM tip were blocked by $A\beta_{40}$ oligomer, the binding probability decreased to 3.5% (blue column, pillar III). Meanwhile, the control experiment results (blue, pillar IV and V) also showed similar reduction of the binding probabilities, which were attributed to decrease in binding events. The results confirmed that the rupture force of Apt1-$A\beta_{40}$ oligomer was caused by a specific interaction. Moreover, for the interaction of Apt1-$A\beta_{40}$ fibril, Apt2-$A\beta_{40}$ oligomer and Apt2-$A\beta_{40}$ fibril, the same conclusion could be achieved. Besides, the interactions of Apt1-$A\beta_{40}$ monomer and Apt2-$A\beta_{40}$ monomer were measured by SMFS. The low binding probability of Apt1-$A\beta_{40}$ monomer (gray column, pillar I in Figure S4A) and Apt2-$A\beta_{40}$ monomer (black column, pillar I in Figure S4A) were similar to the result from control experiments, indicating that there was no specific interaction between Apts and $A\beta_{40}$ monomer (Figure S4B and S4C). In brief, the results clearly verified the specific interaction of Apts and $A\beta_{40}$ aggregates.

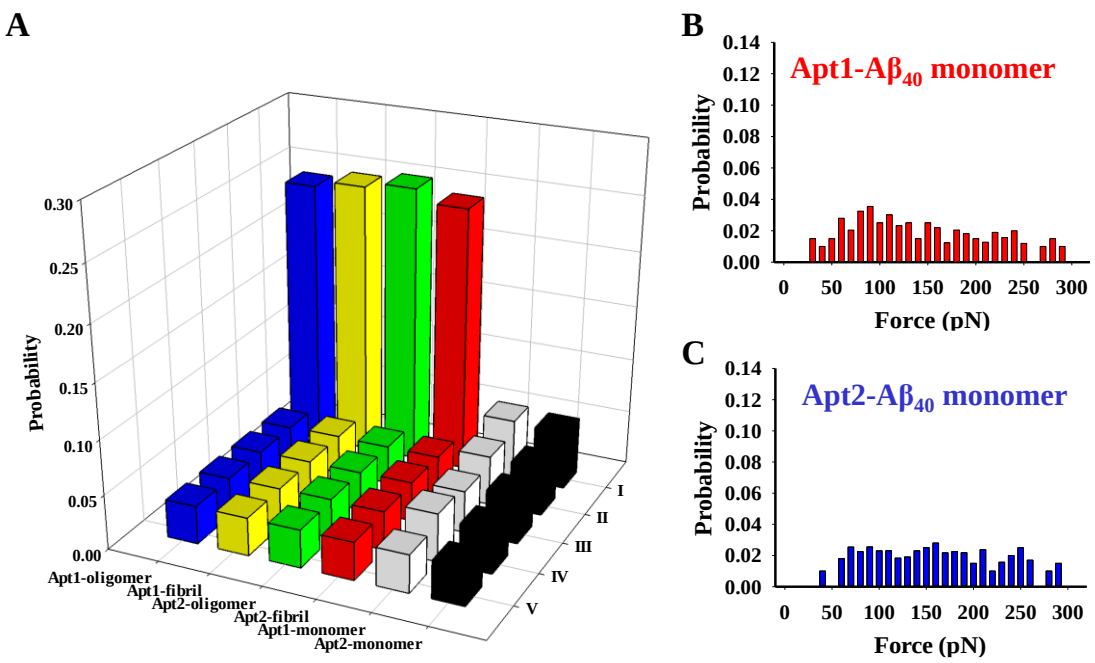

Figure S4. (A) Histogram of binding probabilities of Apt1-Aβ40 oligomer (blue column), Apt1-Aβ40 fibril (yellow column), Apt2-Aβ40 oligomer (green column), Apt 2-Aβ40 fibril (red column), Apt1-Aβ40 monomer (gray column) and Apt2-Aβ40 monomer (black column) at different conditions: (I) Apt1 (or Apt2) modified AFM tip-Aβ40 aggregates (or monomer) modified Au film; (II) Apt1 (or Apt2) modified AFM tip-Aβ40 aggregates (or monomer) modified Au film, and the Au film blocked with Apt1 (or Apt2); (III) Apt1 (or Apt2) modified AFM tip-Aβ40 aggregates (or monomer) modified Au film, and the AFM tip blocked with Aβ40 aggregates (or monomer); (IV) PEG modified AFM tip-Aβ40 aggregates (or monomer) modified Au film; (V) Apt1 (or Apt2) modified AFM tip-bare Au film. (B) Force measurements of Apt1-Aβ40 monomer. (C) Force measurements of Apt2-Aβ40 monomer. The loading rate was 3.52×10^4 pN/s.

S-6 Binding behaviors of Apts with $A\beta_{40}$ monomer, oligomer and fibril

SPR was used to investigate the binding behaviours of Apts with $A\beta_{40}$ monomer and $A\beta_{40}$ aggregates. In brief, 5 μM of thiol-modified Apt was immobilized on the cleaned bare Au film. After the modified Au film was blocked with MCU, then different concentrations (from 0 μM to 50 μM) of $A\beta_{40}$ monomer, $A\beta_{40}$ oligomer, $A\beta_{40}$ fibril, $A\beta_{42}$ monomer, $A\beta_{42}$ oligomer or $A\beta_{42}$ fibril were added and incubated for 1 hour. The SPR spectra were recorded after the Au film was washed with TBS buffer. As shown in Figure S5, there was no shift of SPR resonance angle when the $A\beta_{40}$ monomer was added and incubated. However, the observed resonance angle shift ($\Delta\theta$) increased with an increase in concentration of $A\beta_{40}$ oligomer or $A\beta_{40}$ fibril. The results suggested that Apt1 and Apt2 could not bind $A\beta_{40}$ monomer, while either of them could recognize $A\beta_{40}$ oligomer and $A\beta_{40}$ fibril with different recognition capabilities. Moreover, the SPR signal caused by the interaction between Apt1 and $A\beta_{40}$ aggregates was different from that between Apt2 and $A\beta_{40}$ aggregates.

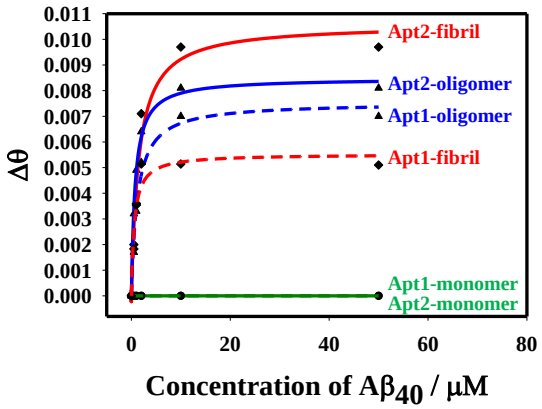

Figure S5. Investigation of the interactions of Apts with $A\beta_{40}$ monomer, oligomer and fibril using SPR. The dash line represented that Apt1 was modified on the Au film, and the solid line represented that Apt2 was modified on the Au film.

S-7 Feasibility of dual Apts-based SPR sensor for detecting $A\beta_{40}$ fibril

The feasibility of dual Apts-based SPR sensor for detecting $A\beta_{40}$ fibril was investigated. As shown in Figure S6A, when the mixed solution of 5 μM $A\beta_{40}$ fibril and random DNA2 functionalized AuNPs was incubated with the Apt2 coated Au film for 30 minutes, SPR spectrum shifted from curve 1 to curve 2 and almost no SPR response was observed. However, when the mixed solution of 5μM $A\beta_{40}$ fibril and Apt1 functionalized AuNPs was incubated with Apt2 coated Au film for 30 minutes, the obvious resonance angle shift (0.1290^{o}) was observed (from curve 2 to curve 3). It suggested that the $A\beta_{40}$ fibril and Apt1 functionalized AuNPs were captured through specific recognition. When 0.1% SDS/10 mM NaOH was introduced for 10 minutes, SPR spectrum shifted from curve 3 to curve 4. The resonance angle of curve 4 was basically consistent with that of curve 1, implying that the sensor chip could be regenerated. In addition, as shown in Figure S6B, the SPR signal kept unchanged when the mixed solution of $A\beta_{40}$ fibril and Apt1 functionalized AuNPs was added and incubated with random DNA1 modified Au film. It indicated that the Apt2 rather than random DNA1 could capture $A\beta_{40}$ fibril and induce the change of SPR signal. The results showed the admirable specificity of established biosensor and the proposed dual Apts-based SPR sensor was feasible.

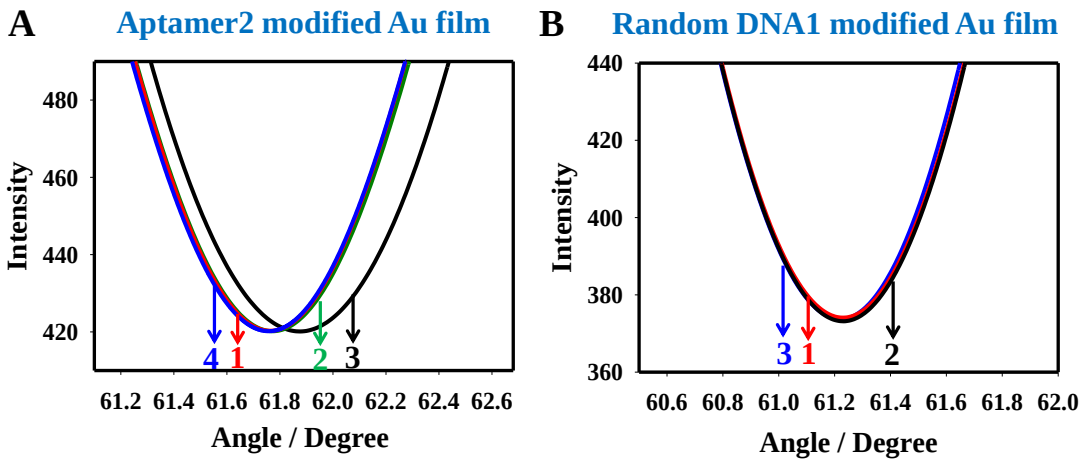

Figure S6. (A) SPR spectra of (1) Apt2 modified Au film; (2) reaction with the mixed solution of $A\beta_{40}$ fibril and random DNA2 functionalized AuNPs; (3) reaction with the mixed solution of $A\beta_{40}$ fibril and Apt1 functionalized AuNPs; (4) regeneration. (B) SPR spectra of (1) random DNA2 modified Au film; (2) reaction with the mixed solution of $A\beta_{40}$ fibril and Apt1 functionalized AuNPs; (3) regeneration.

S-8 Binding behaviors of Apts with Aβ$_{42}$ oligomers using SPR

Take Aβ$_{42}$ oligomer for an example, the binding behaviors of Apts with Aβ$_{42}$ aggregates were also investigated using SPR. In brief, 5 μM of thiol-modified Apt1 (or Apt2) was immobilized on the cleaned bare Au film. After the modified Au film was blocked with 6-mercapto-1-hexanol (MCH), different concentrations (from 0 μM to 100 μM) of Aβ$_{42}$ oligomer was added and incubated for 1 hour. The SPR spectrum were recorded after the Au film was washed with TBS buffer. As shown in Figure S7A, the observed resonance angle shift (Δθ) increased with an increase in concentration of Aβ$_{42}$ oligomer, suggesting that Apt1 and Apt2 could respectively bind Aβ$_{42}$ oligomer. In addition, after Apt2 modified Au film was blocked with MCH (from curve 1 to curve 2), the pre-incubated reaction solution of 10 μM Aβ$_{42}$ oligomer and 10 μM Apt1 was added and incubated for 1 hour As shown in Figure S7B, SPR resonance angle almost kept unchanged (from curve 2 to curve 3), indicating that the simultaneous binding of Apt1 and Apt2 in the presence of Aβ$_{42}$ oligomer not happen.

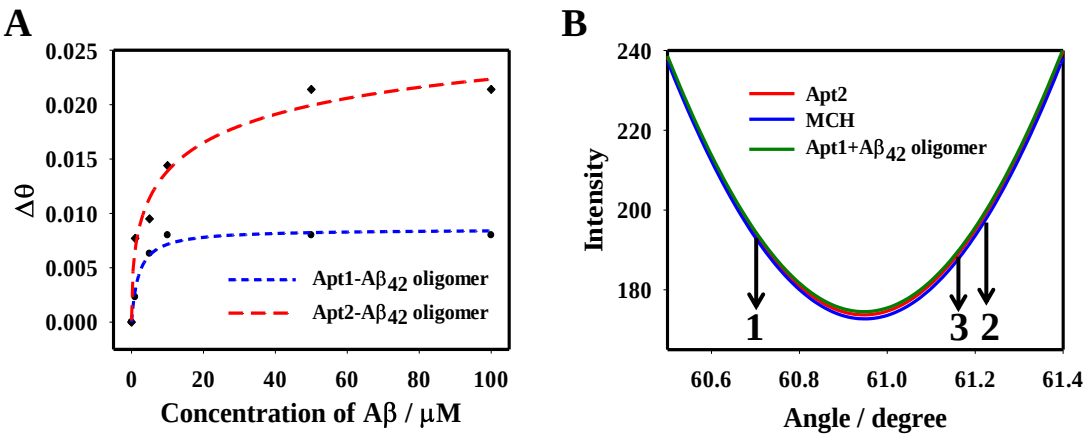

Figure S7. (A) The changes of resonance angle caused by Aβ$_{42}$ oligomers. (B) The SPR spectra of (1) the Apt2 modified Au film; (2) the MCH blocked Apt2-modified Au film; (3) reaction with the pre-incubated reaction solution of Aβ$_{42}$ oligomer and Apt1.

S-9 Detection of Aβ$_{40}$ fibril by dual Apts-based SPR sensor

Dual Apts-based SPR sensor was used for detecting different concentrations of Aβ$_{40}$ fibril in TBS buffer. Figure S8A showed the resonance angle gradually increased as the Aβ$_{40}$ fibril concentration increased from 0 to 10 pM. Figure S8B demonstrated the relation between Δθ and the concentration of Aβ$_{40}$ fibril in two methods (direct measurement and dual Apts-based SPR). It was estimated that the detection limit of dual Apts-based SPR sensor for Aβ$_{40}$ fibril was 0.05 pM (curve a of Figure S8B). Moreover, a comparison between the present work and previously reported studies was performed (shown in Table S2), and the sensitivity of this sensor was comparable to or better than that of those previous works. The result from Figure 6C clearly showed the specificity of the dual Apts-based SPR sensor. Take 5 pM sample as example, Δθ was 0.1246^{o} for Aβ$_{40}$ oligomer, which was twenty-four times larger than that of Aβ$_{42}$ oligomer and sixteen times larger than that of Aβ$_{42}$ fibril. The results demonstrated that this biosensor had sequence specificity to distinguish among Aβ species. As shown in Figure S8C, the reproducibility of the sensor chip was also estimated. When the dual Apts-based SPR sensor was used to detect 1 pM Aβ$_{40}$ fibril, no significant signal degradation was observed during the 6 cycles, implying that the dual Apts-based SPR sensor exhibited good reproducibility.

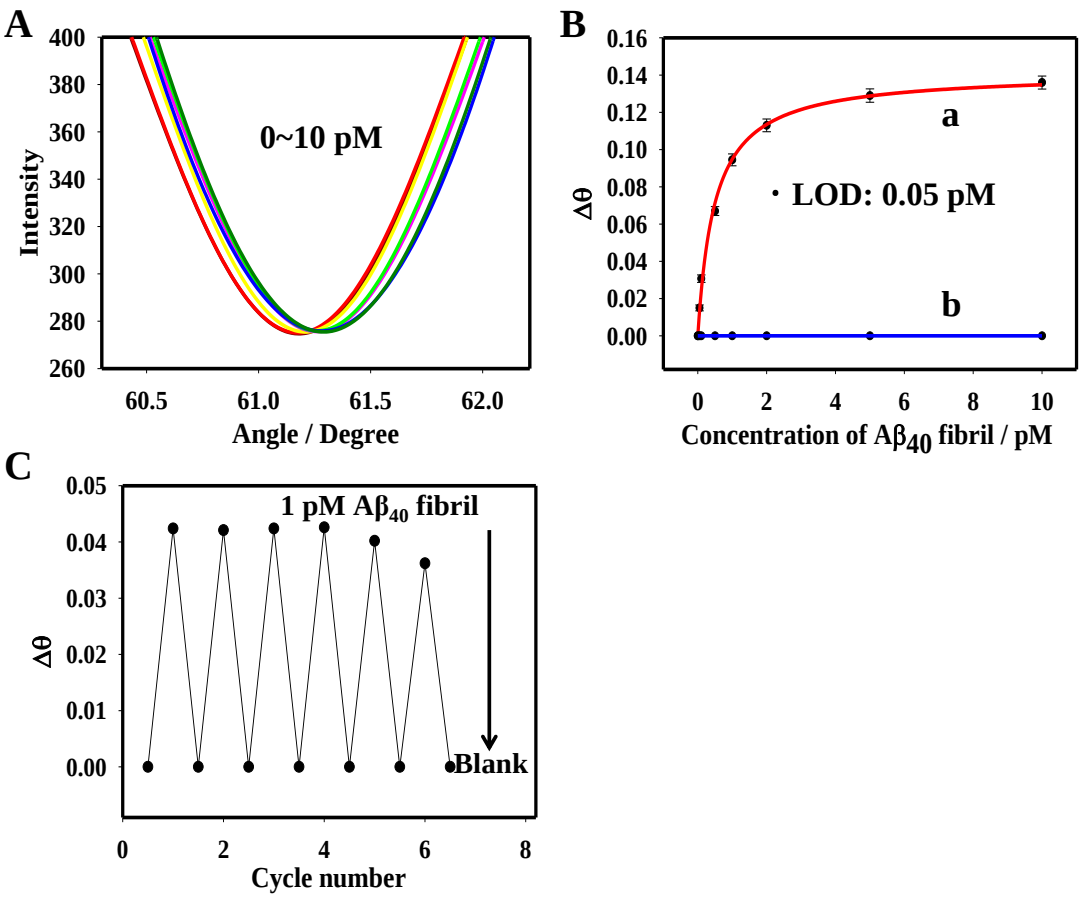

Figure S8. (A) SPR spectra of different concentrations of $A\beta_{40}$ fibrils. (B) Sensitivity investigation of the biosensor. (a) dual Apts-based SPR, (b) direct measurement. (C) Reproducibility investigation of dual Apts-based SPR sensor.

S-10 A brief introduction for detection of Aβ aggregates

An overview on methods for determination of Aβ aggregates was presented in **Table S2**. According to the comparison result, the sensitivity of dual Apts-based SPR sensor was comparable to or better than that of those previous works.

Table S2 Comparison of reported biosensors for Aβ aggregates detection

Methods	**Analytes**	**Limit of detection**	Ref.
Surface-based fluorescence intensity distribution analysis	Aβ oligomers	16 fM	8
Enzyme-linked immunoassay	Aβ oligomer	5 pM	9
Differential pulse voltammetry	Aβ oligomers	100 pM	10
Upconversion fluorescent sensor	Aβ oligomers	36 pM	11
Light-up nonthiolated aptasensor	Aβ oligomers	10 nM	7
Visual and fluorescent assays	Aβ oligomers	0.5 nM for visual assay; 0.2 nM for fluorescent detection	12
Time resolved luminescence resonance energy transfer	Aβ oligomers, fibrils	0.06 μM	13
Förster resonance energy transfer	Aβ oligomers, fibrils	-	14
Immuno-infrared-sensor	Aβ oligomers, fibrils	-	15
Dual Apts-based SPR sensor	Aβ oligomers, fibrils	0.2 pM for Aβ oligomers 0.05 pM for Aβ fibrils	this work

Reference:

1. Tsukakoshi, K.; Abe, K.; Sode, K.; Ikebukuro, K. *Anal. Chem*. **2012**, 84, 5542-5547.

2. Li, Y.; Xu, D.; Ho, S. L.; Li, H. W.; Yang, R.; Wong, M. S. *Biomaterials* **2016**, 94, 84-92.

3. Zheng, Y.; Wang, Q.; Yang, X. H.; Nie, W. Y.; Zou, L. Y; Liu, X. F.; Wang, K. M. Aptamer as a tool for investigating the effects of electric field on $A\beta_{40}$ monomer and aggregates using single-molecule force spectroscopy. *Anal. Chem*. **2019**, 91, 1954-1961.

4. Deng, C. Y.; Liu, H.; Zhang, M. M.; Deng, H. H.; Lei, C. Y.; Shen, L.; Jiao, B.; Tu, Q. Y.; Jin, Y.; Xiang, L.; Deng, W.; Xie, Y. F.; Xiang, J. Light-up nonthiolated aptasensor for low-mass, soluble amyloid-β_{40} oligomers at high salt concentrations. *Anal. Chem.* **2018**, *90*, 1710-1717.

5. Grabar, K. C.; Freeman, R. G.; Hommer, M. B.; Natan, M. J. Preparation and Characterization of Au Colloid Monolayers. *Anal. Chem.* **1995**, 67, 735-743.

6. Wang, Q , Yang, L. J.; Yang, X. H.; Wang, K. M.; He, L. L.; Zhu, J. Q. Electrochemical biosensors for detection of point mutation based on surface ligation reaction and oligonucleotides modified gold nanoparticles. *Anal. Chim. Acta.* **2011**, 688, 163-167.

7. Wang, Q.; Huang, J.; Yang, X. H; Wang, K. M.; He, L. L.; Li, X. P.;Xue, C. Y. Surface plasmon resonance detection of small molecule using split aptamer fragments. *Sensor. Actuat B: Chem*. **2011**, 156, 893-898.

8. Kravchenko, K.; A. Kulawik, M. Hülsemann, K. Kühbach, C. Zafiu, Y. Herrmann, C. Linnartz, L. Peters, T. Bujnicki, J. Willbold, O. Bannach, D. Willbold, Analysis of anticoagulants for blood-based quantitation of amyloid β oligomers in the sFIDA assay, *Biol. Chem.* **2017**, 398, 465-475.

9. Olajos, G.; Bartus, E.; Schuster, I.; Lautner, G.; Gyurcsányi, R. E.; Szogi, T.; Fulop,

L.; Martinek, A. T. Multivalent foldamer-based affinity assay for selective recognition of Aβ oligomers. *Anal. Chim. Acta.* **2017**, *960,* 131-137.

10. Zhou, Y. L.; Zhang, H. Q.; Liu, L. T.; Li, C. M.; Chang, Z.; Zhu, X.; Ye, B. X.; Xu, M. T. Fabrication of an antibody-aptamer sandwich assay for electrochemical evaluation of levels of β-amyloid oligomers. *Sci. Rep*. **2016**, 6, 35186.

11. Jiang, L. F.; Chen, B. C.; Chen, B.; Li, X. J.; Liao, H. L.; Huang, H. M.; Guo, Z. J.; Zhan, W. Y.; Wu, L. Detection of Aβ oligomers based on magnetic-field-assisted separation of aptamer-functionalized Fe_3O_4, magnetic nanoparticles and $BaYF_5$:Yb,Er nanoparticles as upconversion fluorescence labels. *Talanta* **2017**, 170, 350-357.

12. Xia, N.; Zhou, B.; Huang, N.; Jiang, M.; Zhang, J.; Liu, L. Visual and fluorescent assays for selective detection of beta-amyloid oligomers based on the inner filter effect of gold nanoparticles on the fluorescence of CdTe quantum dots. *Biosens. Bioelectron.* **2016**, *85*, 625-632.

13. Pihlasalo, S.; Deguchi, T.; Virtamo, M.; Jacobino, J.; Chary, K.; Francisco R. A. L; Brunhofer-Bolzer, G.; Huttunen, R.; Fallarero, A.; Vuorela, P.; Harma, H. Luminometric nanoparticle-based assay for high sensitivity detection of β-amyloid aggregation. *Anal. Chem.* **2017**, 89, 2398-2404.

14. Alies, B.; Eury, H.; Essassi, E. M.; Pratviel, G.; Hureau, C.; Faller, P. Concept for simultaneous and specific in situ monitoring of amyloid oligomers and fibrils via forster resonance energy transfer. *Anal. Chem.* **2014**, 86, 11877-11882.

15. Nabers, A.; Ollesch, J.; Schartner, J.; Kotting, C.; Genius, J.; Hafermann, H.; Klafki, H.; Gerwert, K.; Wiltfang, J. Amyloid-β-secondary structure distribution incerebrospinal fluid and blood measured by an immuno-infrared-sensor: a biomarker candidate foralzheimer's disease. *Anal. Chem.* **2016**, 88, 2755-2762.